Ultrafast three-dimensional imaging system based on phase-shifting method and hybrid dispersion laser scanning

IEEE Photonics Journal
An IEEE Photonics Society Publication

Open Access

Ultrafast Three-Dimensional Imaging System Based on Phase-Shifting Method and Hybrid Dispersion Laser Scanning

Volume 7, Number 3, June 2015

Bo Dai, Member, IEEE
Dong Wang
Qi Wang
Ruijin Hong
Dawei Zhang
Songlin Zhuang
Xu Wang, Senior Member, IEEE

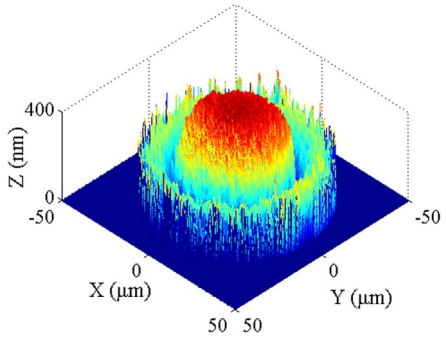

DOI: 10.1109/JPHOT.2015.2428248
1943-0655 © 2015 IEEE

IEEE photonics SOCIETY

IEEE

Ultrafast Three-Dimensional Imaging System Based on Phase-Shifting Method and Hybrid Dispersion Laser Scanning

Bo Dai,[1] *Member, IEEE*, Dong Wang,[1] Qi Wang,[1] Ruijin Hong,[1] Dawei Zhang,[1] Songlin Zhuang,[1] and Xu Wang,[2] *Senior Member, IEEE*

[1]Engineering Research Center of Optical Instrument and System, Ministry of Education, Shanghai Key Laboratory of Modern Optical System, University of Shanghai for Science and Technology, Shanghai 200093, China
[2]Institute of Photonics and Quantum Sciences, School of Engineering and Physical Sciences, Heriot-Watt University, Edinburgh EH14 4AS, U.K.

DOI: 10.1109/JPHOT.2015.2428248

Manuscript received March 5, 2015; revised April 25, 2015; accepted April 27, 2015. Date of publication April 30, 2015; date of current version May 13, 2015. This work was supported in part by the National Science Instrument Important Project under Grant 2012YQ1700047 and Grant 2013YQ16043903, by Pujiang Project of Shanghai Science and Technology Commission under Grant 14PJ1406900, and by the National Natural Science Foundation of China under Grant 61378060. Corresponding author: B. Dai (e-mail: lioneldai2014@163.com).

Abstract: In this paper, we proposed an ultrafast 3-D imaging system based on phase-shifting method and a hybrid dispersion scanning technique. The imaging system is capable of acquiring the 3-D shape of the object at an ultrafast scan rate. A theoretical model is built to describe the operation principle of the imaging system and to analyze the performance of the system. In the demonstration, the imaging system is designed with practical devices and components. The system has a scan rate of 25 MHz and a frame rate of 100 kHz. The field of view is 50 μm $\times$ 50 μm, and the number of pixels of one frame is 260 pixel $\times$ 1000 pixel. The reconstructed 3-D image has the peak signal-to-noise ratio (PSNR) of 30.11 dB. The performance of the imaging system is investigated by analyzing the influence of the input beam size and the resolution of the digitizer. The input collimated light with large beam size is preferred for high image quality. Moreover, the depth resolution can be improved by using high-resolution digital signal processing.

Index Terms: Imaging systems, ultrafast measurements.

1. Introduction

Three-dimensional (3-D) imaging techniques are capable of acquiring quantitative 3-D surface shape, which are very important inspection tools for many applications, including industrial measurement, biomedical examination, material investigation and entertainment [1]–[3]. Most modalities of imaging are based on digital fringe projection and phase-shifting methods [4]–[8]. However, fringe pattern switching rate (up to 120 Hz) for a digital-light-processing (DLP) projector significantly limits the speed of image acquisition. To overcome this issue, a 3-D imaging technique equipped with the DLP Discovery technology is proposed to achieve an unprecedented frame rate of 667 Hz [9].

In addition, imaging techniques employing phase-shifting method can realize accurate measurement because phase-shifting method can be used in the pixel-level measurement

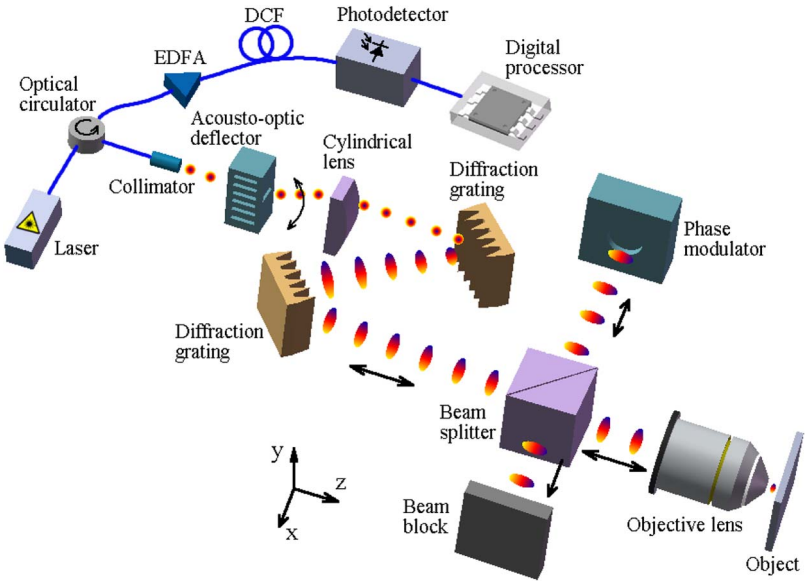

Fig. 1. Schematic diagram of the proposed ultrafast 3-D imaging system.

[9]–[12]. During the 3-D measurement using phase-shifting method, the shape of the object can be measured point by point individually. Besides, surface reflectivity variations of the object do not have influence over the measurement, so the method can be used to measure complex structures. Since the phase-shifting method has less sensitivity to the ambient light, no strict measurement environment is required. Numerous algorithms have been put forward for phase-shifting method, including three-step algorithm, four-step algorithm, Carré algorithm, Hariharan algorithm and least-square algorithm [4], [13]–[16]. The phase-shifting method could be a promising approach for real-time 3-D imaging.

Notwithstanding the dramatic development of the 3-D imaging, accurate acquisition of 3-D information with real-time capability is still a great challenge. Hybrid dispersion laser scanning is a detection technique, which can be used to capture dynamic phenomenon at a great high speed ($>$ 100 MHz and potentially even higher) [17]–[23]. By employing space-to-wavelength mapping and wavelength-to-time mapping, an ultrafast event can be detected by using a single-pixel photodetector with a high temporal resolution. An ultrafast surface vibrometry was demonstrated at a frame rate of 105.4 kHz [18], in which a Michelson interferometry was used to capture the rapid variation of phase profiles resulted from the vibration. In the signal processing, the high-frequency phase profile corresponding to the rapid vibration was retained after the high-pass filtering and used for the calculation of the vibration. However, the vibrometry cannot measure the height of flat surface, because the phase profile corresponding to the flat surface becomes constant and would be removed by the high-pass filter. Thus, it limits the application of vibrometry for 3-D imaging.

In this paper, an ultrafast 3-D imaging technique is proposed, combining the advantageous features of both phase-shifting method and hybrid dispersion laser scanning. The proposed technique is capable of acquiring the 3-D profile, whatever the object has a complex surface or is a flat platform, at an ultrafast frame rate.

2. Operation Principle

The schematic diagram of the proposed ultrafast 3-D imaging system is shown in Fig. 1. A short pulse with broadband spectrum from a femtosecond pulse laser is fed into an optical circulator. The output from Port 2 of the optical circulator is collimated by a collimator and fed into an acousto-optic deflector (AOD), which deflects the light in the y-dimension. A cylindrical lens collimates the deflected light. A pair of gratings disperses the light along the x-dimension so that the light with different wavelengths is mapped into different positions in the x-dimension.

The electrical field (E-field) of the dispersed light can be expressed as follows:

$$E_D(x,\lambda) = E_{\text{in}}(\lambda)\exp\left[-\left(\frac{x-\Delta x(\lambda)}{W_D}\right)^2\right]$$

where $\Delta x(\lambda)$ is the spatial separation of the light at a certain wavelength λ to that at the peak wavelength, λ_0.

The spatial separation is determined by the grating dispersion characteristics. W_D is the beam size of dispersed light (the radius where intensity falls to $1/e^2$), which is almost same as the input collimated beam size, W_{in}. $\Delta x(\lambda)$ can be defined as follows:

$$\Delta x(\lambda) = \cos(\theta_{\text{in}})P\left\{\tan\left(\sin^{-1}(\lambda/d - \sin(\theta_{\text{in}}))\right) - \tan\left(\sin^{-1}(\lambda_0/d - \sin(\theta_{\text{in}}))\right)\right\}$$

where E_{in} is the amplitude of the input light, d is the grating period, θ_{in} is the incident angle of the collimated light into the grating, and P is the perpendicular distance between the gratings.

Then, the light is split into two paths by a beam splitter. One is the signal optical path and the other is reference optical path. In the reference optical path, the light is modulated by a phase modulator in a time-multiplexing manner with a set of phases $\{\delta(m)\}$ every M successive optical pulses, where $m = 1, 2, \ldots, M$ and M is the step number of phase-shifting method. The E-field of the mth spatially dispersed modulated pulse is

$$E_r(x,\lambda,m) = \frac{1}{2}E_D(x,\lambda)\exp[j(\phi_r(x,\lambda) - \delta(m))]$$

where $\phi_r(x,\lambda)$ is the phases of the reference light.

In the signal optical path, the light illuminates the object via an objective lens. (The use of the objective lens is optional.) If the objective lens is used, the dispersed spatial position of the light and the beam size of the dispersed light can be rewritten as follows:

$$\Delta x(\lambda)_{\text{Objective}} = \Delta x(\lambda)/MF, \qquad W_{\text{Objective}} \approx \frac{4\lambda f}{\pi W_{\text{in}}}$$

where MF is the magnification factor of the objective lens, and f is the focal length of the objective lens.

The E-filed of the light after illuminating the object is

$$E_t(x,\lambda) = \frac{\alpha(x,\lambda)}{2}E_D(x,\lambda)\exp[j(\phi_r(x,\lambda) + \phi_h(x,\lambda))]$$

where $\alpha(x,\lambda)$ is the loss of the light corresponding to the surface reflectivity of the object, and $\phi_h(x,\lambda)$ is the phase shift resulted from the height of the object, and it can be expressed in terms of the height

$$\phi_h(x,\lambda) = \frac{4\pi h(x,\lambda)}{\lambda}.$$

The signals from two optical paths are combined and interfere with each other. The E-field of the interfered light, $E_i(x,\lambda,m)$, is the sum of the light from the two optical paths, and the intensity of the interfered light is

$$I(x,\lambda,m) = |E_i(x,\lambda,m)|^2 = |E_r(x,\lambda,m) + E_t(x,\lambda)|^2 = I'(x,\lambda) + I''(x,\lambda)\cos[\phi_h(x,\lambda) + \delta(m)]$$

where $I'(x,\lambda)$ is the average intensity, $I'(x,\lambda) = [1 + \alpha(x,\lambda)]E_D^2(x,\lambda)/2$ and $I''(x,\lambda)$ is the fringe modulation, $I''(x,\lambda) = \alpha(x,\lambda)E_D^2(x,\lambda)/2$. These two parameters have no influence over the height reconstruction. It indicates that in the proposed system the surface reflectivity of the object has no influence over the 3-D imaging.

The interfered light is output from Port 3 of the optical circulator and amplified by an erbium doped fiber amplifier (EDFA). A dispersive optical fiber is followed to stretch the optical signal in time domain to realize wavelength-to-time mapping. Considering large group-velocity dispersion (GVD) and ignoring nonlinearity and polarization-mode dispersion, the wavelength-to-time mapping can be described as [24]–[26]

$$\tau(\lambda) = \beta_2 L\left(\frac{2\pi c}{\lambda} - \frac{2\pi c}{\lambda_0}\right)$$

where β_2 is the second-order dispersion coefficient, which can be expressed as $\beta_2 = D\lambda_0^2/2\pi c$, c is velocity of light in vacuum, D is the dispersion coefficient of the dispersive fiber, and L is the length of the dispersive fiber.

By means of space-to-wavelength mapping and wavelength-to-time mapping, the spatial information (xy-plane) of the object is mapped into time domain. Then, a single-pixel photodetector is used to realize optical-to-electrical conversion. The height information of the object is extracted from measuring every M successive dispersed pulses using phase-shifting method.

In the proposed imaging system using M-step phase-shifting method, the line scan rate sacrifices for the phase modulation and becomes $1/M$ of the repetition rate, R, i.e., R/M. In practice, owing to the redundancy of the data, the scan rate of the AOD, r, is much smaller than the line scan rate, R/M, and thus the frame rate and the number of pixels are not affected [18]. The frame rate is determined by the scan rate of the AOD, r. The number of pixels is given by

$$N_x \times N_y = (DLf_{\text{dig}}\Delta\lambda) \times (R/r)$$

where f_{dig} is the sampling rate of the digital processor.

3. Demonstration of the Ultrafast 3-D Imaging System

Based on the theoretical model, we demonstrate the operation of the proposed ultrafast 3-D imaging system. In the demonstration, optical short pulses have the pulse width of 90 fs full width at half maximum (FWHM). The center wavelength of the light is 1550 nm and the -3 dB bandwidth is 20 nm. The repetition rate of the laser, R, is 100 MHz. The beam size after the optical collimator is 5 mm (the radius where intensity falls to $1/e^2$). The AOD has the scan rate of 100 kHz and acousto-optic bandwidth of 100 MHz. The groove density of the grating pair is 600 lines/mm and the incident angle is 35°. The phase modulator has the modulation rate of 100 MHz. The phases used in the phase modulation are $(0, \pi/2, \pi, 3\pi/2)$ for every four successive pulses. The magnification factor of the objective lens is 50×. The length of the dispersion compensation fiber (DCF) is 5 km and the dispersion coefficient, D, is -130 ps/nm · km. The bandwidth of the photodetector is 12 GHz, which is commercially available. The digital processor has 4 GHz bandwidth and 20 GS/s sampling rate. The resolution of the analog-to-digital conversion (ADC) is 10-bit.

Four-step phase-shifting method is used in the demonstration. Fig. 2(a) illustrates the object used in the demonstration, which has the size of about 50 μm × 50 μm and the height of 400 nm. The object has very complex shape. Fig. 3 shows a cross section of the object and the red solid line is the contour of the target. In the demonstration, four Gaussian-shaped optical pulses are spatially dispersed and split into two branches sequentially. In the one branch, the optical pulses are to collect the contour of the target every 10 ns, while the optical pulses in the other branch are phase-modulated by $\delta(m) = 0$, $\pi/2$, π, and $3\pi/2$. After image acquisition and phase modulation, the optical pulses are reflected back and coupled into the fiber via Port 3 of the optical circulator. Interference occurs when the light from the two branches combines together. Then, the light is temporal dispersed in the DCF for wavelength-to-time mapping. The information in the spectrum can be read out from the waveform in the time domain. The single-pixel

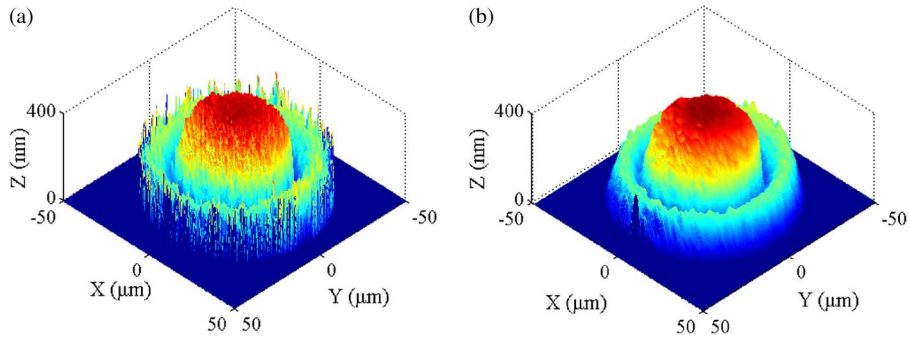

Fig. 2. (a) Object of complex shape used in the demonstration and (b) reconstructed 3-D image when the input beam size is 5 mm.

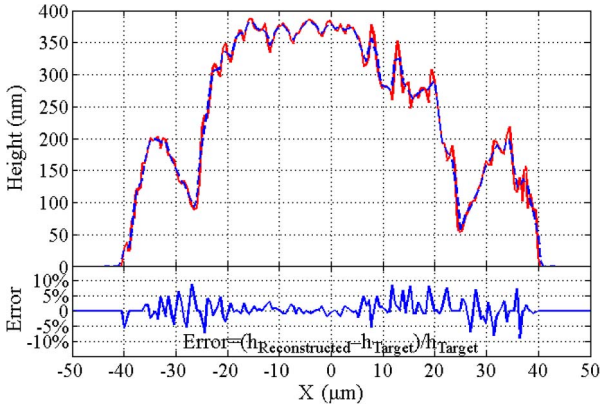

Fig. 3. Contour of the target.

photodetector is used for optical-to-electrical conversion. In the signal processing, the contour of the target can be reconstructed by using the four-step phase-shifting method. The relationship between the height of the object and the intensities of the four successive pulses is expressed as follows:

$$h(x,\lambda) = \frac{\lambda}{4\pi}\tan^{-1}\left[\frac{I(x,\lambda,4) - I(x,\lambda,2)}{I(x,\lambda,1) - I(x,\lambda,3)}\right].$$

By calculating the intensities of the four successive dispersed pulses, the contour of the target can be reconstructed, as shown in Fig. 3 (blue dashed line). The reconstructed contour agrees with the target well. The deviation between the reconstructed contour and the target is within ±10%, as illustrated in Fig. 3. By scanning the object along y-direction, the shape of the whole object can be reconstructed. The reconstructed 3-D image is depicted in Fig. 2(b). The reconstructed 3-D image matches the original object well. Comparing with the original object, the reconstructed image has the root-mean-square-error (RMSE) of 12.49 nm and the peak signal-to-noise ratio (PSNR) of 30.11 dB.

Then, the proposed ultrafast 3-D imaging system is demonstrated to reconstruct flat platforms. The object is shown in Fig. 4(a). The four flat platforms have the height of 0, 100, 200, and 400 nm, respectively. The height of the platforms is abruptly changed. The system parameters are kept the same as those in the previous demonstration. The reconstructed 3-D image is shown in Fig. 4(b). The four platforms are reconstructed. The height of the platforms is almost unchanged, except that the height of the highest platform becomes 393.4 nm. The edges of the platforms have slight transition. The RMSE and PSNR of the reconstructed image are 10.71 nm and 30.3 dB.

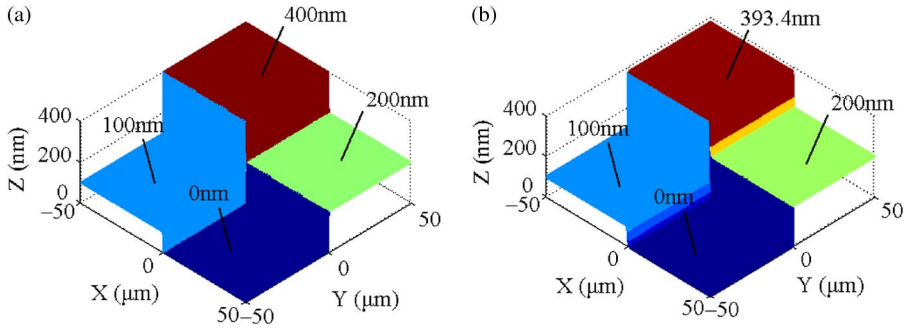

Fig. 4. (a) Flat platforms used in the demonstration. (b) Reconstructed 3-D image when the input beam size is 5 mm.

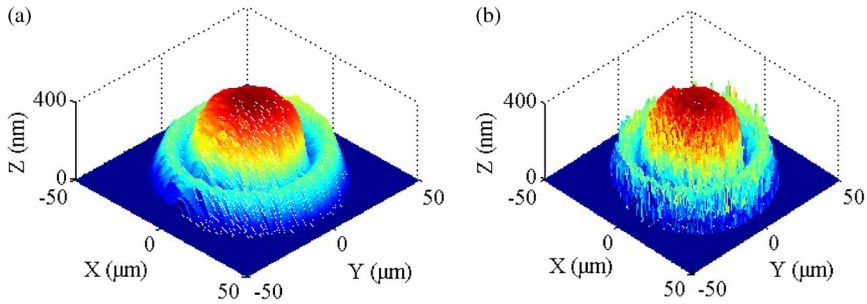

Fig. 5. Reconstructed 3-D images when the input beam size is (a) 2 mm and (b) 10 mm.

In the demonstration, the line scan rate is one-fourth of the repetition rate of the laser, i.e., 25 MHz. The frame rate is 100 kHz. The field of view is 50 μm $\times$ 50 μm. The number of pixels of one frame is 260 pixel $\times$ 1000 pixel. The proof-to-concept demonstrations realize the ultrafast 3-D image reconstruction of the complex-shape and flat-platform objects.

4. Performance of the Ultrafast 3-D Imaging System

4.1. Image Quality

In the proposed 3-D imaging system, the shape of the object is measured in the pixel-level. Each point of the object is mapped to wavelength and time point-by-point. The quality of the height reconstruction is also affected by the spatial resolution. It is straightforward to improve the spatial resolution by changing the input beam size. When the input beam size is increased, the spot size of the light illuminating on the object becomes small. If the spot size is small, the light at a certain wavelength acquires the image of a specific position and the circumjacent image as interference has less influence on the modulation of the light, realizing the point-by-point measurement. Besides, the space-to-wavelength mapping presents a linear fashion. The change of the beam size does not affect the diffraction of the light with different wavelengths.

Fig. 5 illustrates the reconstructed 3-D image when the input collimated beam has the beam size of 2 mm and 10 mm (the radius where intensity falls to $1/e^2$). When the input beam size is small, the spot size of the light illuminating on the object is large. Therefore, the light is not only modulated with the spatial information at specific position but modulated with the circumjacent shape of the object as well, which causes interference to height reconstruction. The reconstructed 3-D image has smooth profile and the coarse contour of the original object is obtained. If the input beam size of 10 mm is used, the light with very small spot size illuminates a tiny position. The light is mainly modulated with the specific target and the circumjacent shape of the object has little influence over the light modulation. The reconstructed 3-D image is shown in

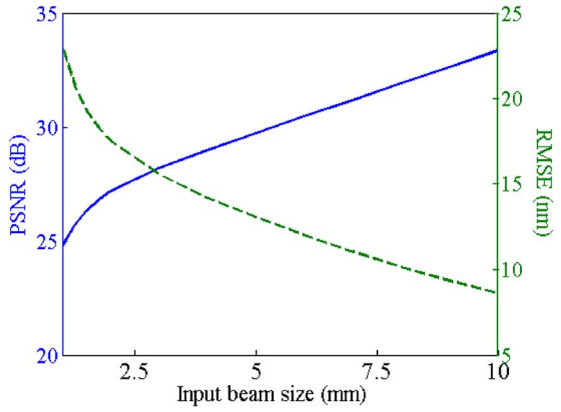

Fig. 6. Relationship between the input beam size and the performance of 3-D imaging system.

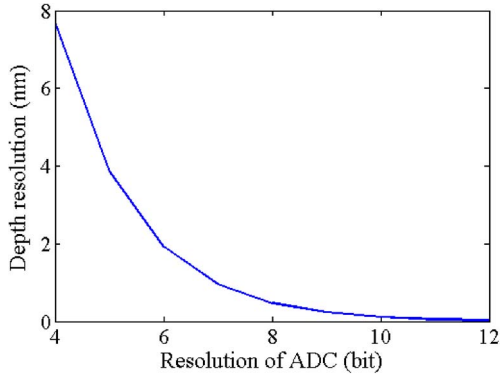

Fig. 7. Relationship between the resolution of ADC and depth resolution.

Fig. 5(b). Details of the original object can be found in the reconstructed image. The performance of the 3-D image reconstruction is acceptable. Fig. 6 shows the PSNR and RMSE of the reconstructed images when the input beams with different beam sizes are used. The low PSNR (< 30 dB) and large RMSE (> 15 nm) indicate lossy reconstruction if the input beam with small beam size is used. With the increase of the input beam size, the PSNR improves and the RMSE is reduced to < 10 nm. The performance of the 3-D image reconstruction becomes better in the absence of the interference.

4.2. Depth Resolution

Depth resolution is an important measure to evaluate the accuracy of the 3-D imaging system. In the proposed imaging system, the depth of object is figured out by calculating the amplitude of the electrical signal in the digital signal processing. The quantization of the electrical signal affects discrimination of the minimum difference of depth. Therefore, the resolution of ADC in the digital signal processing is a key factor to determine the depth resolution. The depth resolution of the imaging system employing four-step phase-shifting method can be calculated as follows:

$$h_{\min} = \frac{\lambda}{4\pi} \tan^{-1}\left[\frac{1}{2^N}\right]$$

where N is the resolution of ADC, i.e., effective number of bits.

Fig. 7 illustrates the relationship of the resolution of ADC and depth resolution. The imaging system can achieve sub-nanometer depth resolution. Moreover, if the resolution of ADC is higher, the capability of digital processing to discriminate the minimum difference of depth becomes

better so that smaller-scale depth resolution can be achieved. For example, the imaging system equipped with the digital processor of the resolution more than 8 bits, which is commercially available, can realize the depth resolution less than 0.48 nm.

5. Conclusion

In conclusion, we have proposed a new ultrafast 3-D imaging system. By employing hybrid dispersion laser scanning technique, the proposed imaging system was capable of scanning an object at an ultra-high scan rate. The adoption of phase-shifting method enabled 3-D shape reconstruction of the object by means of point-by-point measurement. We have developed the theoretical model and simulate the operation principle of the proposed imaging system. With the help of the theoretical model, we have investigated the performance of the imaging system in terms of image quality and depth resolution. High PSNR and low RMSE can be achieved by using large input beam size. High resolution of ADC results in precise discrimination of the minimum difference of depth and the sub-nanometer depth resolution can be realized. The proposed ultrafast 3-D imaging system is capable of measuring any complex and flat profiles and has the potential to be used in the many industrial applications and research work, such as cell observation, material characterization and machinery monitoring.

References

[1] W. J. Mulholland *et al.*, "Multiphoton high-resolution 3-D imaging of Langerhans cells and keratinocytes in the mouse skin model adopted for epidermal powdered immunization," *J. Invest. Dermatol.*, vol. 126, no. 7, pp. 1541–1548, Jul. 2006.
[2] S. V. Aert, K. J. Batenburg, M. D. Rossell, R. Erni, and G. V. Tendeloo, "Three-dimensional atomic imaging of crystalline nanoparticles," *Nature*, vol. 470, no. 7334, pp. 374–377, Feb. 2011.
[3] H. Dohi *et al.*, "Three-dimensional imaging in polymer science: Its application to block copolymer morphologies and rubber composites," *Polymer J.*, vol. 39, no. 8, pp. 749–758, 2007.
[4] D. Malacara, Ed. *Optical Shop Testing*, 3rd ed. New York, NY, USA: Wiley, 2007.
[5] K. Leonhardt, U. Droste, and H. J. Tiziani, "Microshape and rough-surface analysis by fringe projection," *Appl. Opt.*, vol. 33, no. 31, pp. 7477–7488, Nov. 1994.
[6] C. Zhang, P. S. Huang, and F.-P. Chiang, "Microscopic phase-shifting profilometry based on digital micromirror device technology," *Appl. Opt.*, vol. 41, no. 8, pp. 5896–5904, 2002.
[7] S. Lei and S. Zhang, "Flexible 3-D shape measurement using projector defocusing," *Opt. Lett.*, vol. 34, no. 20, pp. 3080–3082, 2009.
[8] S. Zhang, "Recent progresses on real-time 3-D shape measurement using digital fringe projection techniques," *Opt. Laser Eng.*, vol. 48, no. 2, pp. 149–158, Feb. 2010.
[9] S. Zhang, D. V. D. Weide, and J. Oliver, "Superfast phase-shifting method for 3-D shape measurement," *Opt. Exp.*, vol. 18, no. 9, pp. 9684–9689, 2010.
[10] K. Kinnstaetter, A. W. Lohmann, J. Schwider, and N. Streibl, "Accuracy of phase shifting interferometry," *Appl. Opt.*, vol. 27, no. 24, pp. 5082–5089, Dec. 1988.
[11] P. Hariharan, "Phase-shifting interferometry: Minimization of systematic errors," *Opt. Eng.*, vol. 39, no. 4, pp. 967–969, Apr. 2000.
[12] S. Zhang and S. T. Yau, "High-resolution, real-time 3-D absolute coordinate measurement based on a phase-shifting method," *Opt. Exp.*, vol. 14, no. 7, pp. 2644–2649, Apr. 2006.
[13] P. S. Huang and S. Zhang, "Fast three-step phase-shifting algorithm," *Appl. Opt.*, vol. 45, no. 21, pp. 5086–5091, Jul. 2006.
[14] P. Hariharan, B. F. Oreb, and T. Eiju, "Digital phase-shifting interfeometry: A simple error-compensating phase calculation algorithm," *Appl. Opt.*, vol. 26, no. 13, pp. 2504–2506, 1987.
[15] P. L. Wizinowich, "Phase shifting interferometry in the presence of vibration: A new algorithm and system," *Appl. Opt.*, vol. 29, no. 22, pp. 3271–3279, Aug. 1990.
[16] Y. Zhu and T. Gemma, "Method for designing error-compensating phase-calculation algorithms for phase-shifting interferometry," *Appl. Opt.*, vol. 40, no. 25, pp. 4540–4546, Sep. 2001.
[17] K. Goda, K. K. Tsia, and B. Jalali, "Serial time-encoded amplified imaging for real-time observation of fast dynamic phenomena," *Nature*, vol. 458, no. 30, pp. 1145–1150, 2009.
[18] K. Goda *et al.*, "Hybrid dispersion laser scanner," *Sci. Rep.*, vol. 2, no. 445, pp. 1–8, 2012.
[19] T. T. W. Wong *et al.*, "Asymmetric-detection time-stretch optical microscopy (ATOM) for ultrafast high-contrast cellular imaging in flow," *Sci. Rep.*, vol. 4, p. 3656, Jan. 2014.
[20] H. Chen *et al.*, "Ultrafast web inspection with hybrid dispersion laser scanner," *Appl. Opt.*, vol. 52, no. 17, pp. 4072–4076, Jun. 2013.
[21] H. Chen *et al.*, "Multiwavelength time-stretch imaging system," *Opt. Lett.*, vol. 39, no. 7, pp. 2202–2205, Apr. 2014.
[22] F. Xing, H. Chen, S. Xie, and J. Yao, "Ultrafast surface imaging with an increased spatial resolution based on polarization-division multiplexing," *J. Lightw. Technol.*, vol. 33, no. 2, pp. 396–402, Jan. 2015.

[23] F. Xing, H. Chen, M. Chen, S. Yang, and S. Xie, "Simple approach for fast real-time line scan microscopic imaging," *App. Opt.*, vol. 52, no. 28, pp. 7049–7053, Oct. 2013.
[24] K. Goda and B. Jalali, "Dispersive Fourier transformation for fast continuous single-shot measurements," *Nat. Photon.*, vol. 7, pp. 102–112, 2013.
[25] G. P. Agrawal, *Fiber-Optic Communication Systems*. New York, NY, USA: Wiley, 2002, Ch. 7.
[26] M. Khafaji, H. Gustat, F. Ellinger, and C. Scheytt, "General time-domain representation of chromatic dispersion in single-mode fibers," *Photon. Technol. Lett.*, vol. 22, no. 5, pp. 314–316, Mar. 2010.